NASA/TM-20210018453

Non-Causal Controller Approximation Methodology Augmented With Model Reference Control—Robust Design

George Kopasakis
Glenn Research Center, Cleveland, Ohio

July 2021

NASA STI Program . . . in Profile

Since its founding, NASA has been dedicated to the advancement of aeronautics and space science. The NASA Scientific and Technical Information (STI) Program plays a key part in helping NASA maintain this important role.

The NASA STI Program operates under the auspices of the Agency Chief Information Officer. It collects, organizes, provides for archiving, and disseminates NASA's STI. The NASA STI Program provides access to the NASA Technical Report Server—Registered (NTRS Reg) and NASA Technical Report Server—Public (NTRS) thus providing one of the largest collections of aeronautical and space science STI in the world. Results are published in both non-NASA channels and by NASA in the NASA STI Report Series, which includes the following report types:

- TECHNICAL PUBLICATION. Reports of completed research or a major significant phase of research that present the results of NASA programs and include extensive data or theoretical analysis. Includes compilations of significant scientific and technical data and information deemed to be of continuing reference value. NASA counter-part of peer-reviewed formal professional papers, but has less stringent limitations on manuscript length and extent of graphic presentations.

- TECHNICAL MEMORANDUM. Scientific and technical findings that are preliminary or of specialized interest, e.g., "quick-release" reports, working papers, and bibliographies that contain minimal annotation. Does not contain extensive analysis.

- CONTRACTOR REPORT. Scientific and technical findings by NASA-sponsored contractors and grantees.

- CONFERENCE PUBLICATION. Collected papers from scientific and technical conferences, symposia, seminars, or other meetings sponsored or co-sponsored by NASA.

- SPECIAL PUBLICATION. Scientific, technical, or historical information from NASA programs, projects, and missions, often concerned with subjects having substantial public interest.

- TECHNICAL TRANSLATION. English-language translations of foreign scientific and technical material pertinent to NASA's mission.

For more information about the NASA STI program, see the following:

- Access the NASA STI program home page at http://www.sti.nasa.gov

- E-mail your question to help@sti.nasa.gov

- Fax your question to the NASA STI Information Desk at 757-864-6500

- Telephone the NASA STI Information Desk at 757-864-9658

- Write to:
  NASA STI Program
  Mail Stop 148
  NASA Langley Research Center
  Hampton, VA 23681-2199

NASA/TM-20210018453

Non-Causal Controller Approximation Methodology Augmented With Model Reference Control—Robust Design

George Kopasakis
Glenn Research Center, Cleveland, Ohio

National Aeronautics and
Space Administration

Glenn Research Center
Cleveland, Ohio 44135

July 2021

This work was sponsored by the Advanced Air Vehicle Program
at the NASA Glenn Research Center

Level of Review: This material has been technically reviewed by technical management.

Available from

NASA STI Program
Mail Stop 148
NASA Langley Research Center
Hampton, VA 23681-2199

National Technical Information Service
5285 Port Royal Road
Springfield, VA 22161
703-605-6000

This report is available in electronic form at http://www.sti.nasa.gov/ and http://ntrs.nasa.gov/

Non-Causal Controller Approximation Methodology Augmented With Model Reference Control—Robust Design

George Kopasakis
National Aeronautics and Space Administration
Glenn Research Center
Cleveland, Ohio 44135

Abstract

This paper describes the development of a new control design methodology based on a non-causal controller structure and its approximation. The non-causal controller design is based on a loop shaping approach. Partial fraction decomposition is used, along with derivative approximations, to derive a proper transfer function design for a causal control structure. The premise for this non-causal control methodology is that the phase delay as a function of frequency ideally remains within approximately –90°, which tends to make the system robustly stable to uncertainties in the plant dynamics. To have a predictable control system response in lieu of the tolerance of this methodology to relatively large uncertainty in the plant dynamics, the approach is augmented with model reference control. The addition of model reference control can potentially further enhance the robustness of the design. A control system design example is presented in this paper, along with simulation results, to demonstrate the high degree of robustness of this non-causal methodology and its augmentation.

1.0 Introduction

This paper presents a new control design approach based on a non-causal controller design (i.e., a controller with an improper Transfer Function (TF)) along with its causal approximation. The premise for the non-causal controller is developing an Open Loop (OL) TF of one more pole than zero. This is because such a design, if it were realizable, would maintain a 90° Phase Margin (PM) and result in a Root Locus (RL) that will be stable independent of the magnitude of the TF proportional gain or the actual locations of the poles and zeros in the left half-plane (Ref. 1). To make the controller TF realizable or proper, an approximation of the non-causal controller design is developed, with an effort to maintain the stability properties of the non-causal controller. This control methodology exhibits significant robustness especially, for plant proportional gain uncertainty (PPGU). To be able to have predictable control system response for relatively large PPGU, this approach is augmented with Model Reference Control (MRC). The MRC augmentation can potentially increase the robustness of the overall design. For the example presented, stability and performance are maintained with about ± 2 orders of magnitude of plant proportional gain variability, along with significant robustness for the rest of the control system dynamics.

Control system robustness is an area of interest to the control design community, resulting in numerous theoretical and practical research publications during the last few decades. The design approaches investigated in the literature for control system robustness are primarily based on the methods of LQR, LQG, QFT, LQG/LTR, and Mu-synthesis. For these methodologies, assessment of control system robustness is typically limited to a percentage of uncertainty of the plant dynamics, which can vary from values as low as 10 percent, up to around 100 percent (e.g., Refs. 2 to 5). In cases with large uncertainties in plant dynamics, scheduled controllers may be required to cover the entire envelope of operation.

A robust control design approach was published in Reference 6 that is based on a Loop Shaping (LS) design methodology, followed by an RL design, and then MRC design. The non-causal controller approximation approach and its MRC augmentation presented here is similar to that in Reference 6 in terms of the degree of robustness it achieves, but it simplifies the design process by eliminating the need for the RL design steps. Normally, the controller TF is made causal by padding it with high frequency poles (Ref. 6); this process is purposely skipped here. Instead, the non-causal controller is approximated by a causal controller using *partial fraction decomposition* along with derivative approximations.

The non-causal controller is designed using the LS technique published in References 1 and 7. This technique is systematic and can be applied to develop higher order controllers with the ability to take maximum advantage of the actuator speed to improve performance. This is in contrast to the LS techniques found in literature as H∞ control (Refs. 8 and 9), predetermined control structures like PID in Reference 10, or other specific lead-lag compensator structures like in Reference 11. The robustness of the non-causal controller methodology is improved by augmenting it with MRC, which also enables the control system to exhibit predictable response time characteristics by forcing the response to follow a reference model.

The paper is organized as follows. First, a non-causal controller is designed for a control design example. Then, the partial fraction decomposition, that segments the controller TF into sets of proper and improper components, is determined. This section also includes the approximation for the improper TFs together with the results that demonstrate the performance of the new method. Next, the design is augmented with MRC and the overall performance of the design is demonstrated. Finally, some concluding remarks are offered.

2.0 The Non-Causal Controller Design and Approximation

A non-causal controller is one with an improper TF, that is, a TF where the number of zeros, n_z, is greater than the number of poles, n_p. The additional zeros will cause the magnitude of the TF response to grow unbounded with increasing frequency. Reference 1 shows how an OL TF with $n_p = n_z + 1$, can result in a control system design that is theoretically stable to unbounded PPGU. However, physical processes cannot be designed to be infinitely stable to PPGU, as unmodeled dynamics will always be encountered at some point with increasing frequency. This is because an increase in plant proportional gain will cause a proportional increase in the bandwidth of the system, i.e., the crossover frequency where stability properties are defined.

The strategy adopted in this work is to design a control system OL TF with $n_z = n_p - 1$. To this end, the control design approach described in this paper starts with the LS technique described in References 1 and 7. Here, however, the controller design process will be terminated when the number of zeros in the OL TF becomes one less than the corresponding number of poles. This is achieved without adding padding poles to make the controller TF proper. This approach results in a desired RL shape as was discussed in Reference 1, but in most cases (i.e., except for cases where the plant TF is not strictly proper), it results in a non-causal controller. For the cases where the process leads to a non-causal controller, partial fraction decomposition is used to derive a summation of controller components with some components being causal while others are not. The non-causal components are derivative terms. To remedy the non-causal components, the approach here is to approximate the derivative terms by applying low pass (LP) filters. Applying properly designed LP filters to the derivative terms will result in a causal controller structure, while approximately preserving the original non-causal controller design. This satisfies the objective of developing a proper TF for the controller.

2.1 Example Problem

To help explain this non-causal control design methodology, an example problem is entertained. Let the TF representing the plant for this control design example including the plant actuator and a LP filter to reduce wideband noise, be as follows:

$$G_P(\mathrm{s}) = K_p \frac{8.957x10^{12}}{14.78s^7+7982s^6+2.132x10^6s^5+1.845x10^8s^4+5.493x10^9s^3+8.461x10^{10}s^2+3.919x10^{11}s+2.875x10^{11}} \quad (1)$$

The proportional gain, K_p, of this plant varies from a value of 0.5 to 7.5 over the entire operating range. For this example case, the rest of the dynamics of this plant, in terms of damping and frequencies, do not exhibit appreciable variability. One of the requirements in this example is to design a single controller with the ability to handle all the PPGU. Furthermore, the objective is to design a controller that exhibits stable performance and good disturbance rejection over the full range of PPGU (Refs. 1, 6, and 7). Phase and gain margins of 60° and 6 dB, respectively, can be characterized as good stability margins. Furthermore, approximately 20 dB OL gain at mid-frequency (i.e., at 0.1 times the crossover frequency) can be characterized as good noise rejection. Another objective for the control system is to closely follow the time domain response of the following reference model.

$$G_R(s)= \frac{1}{(s/0.9+1)} \quad (2)$$

2.2 The Non-Causal Controller Design

To employ the LS control design methodology (Refs. 1 and 7), a desired OL TF, $G_d(s)$, that reflects the sought-after performance of the Closed Loop (CL) system is needed. Here, $G_d(s)$ is designed so that the CL time domain response matches the time domain response of the reference model, $G_R(s)$, in Equation (2). For this to occur, the 0 dB crossover frequency of $G_d(s)$ will need to be the same as the 3 dB frequency of $G_R(s)$, which is 0.9 rad/s. Considering the potential for a large range of PPGU, the 0.9 rad/s crossover frequency of $G_d(s)$ will be met only for a select proportional gain of the plant—that is the one used to design the controller. However, at the completion of the control design process, MRC is used to force the control system response to meet that of the reference model, $G_R(s)$.

The $G_d(s)$ TF is designed here to have two poles and one zero. Let one pole be located at the origin for zero steady-state error to a step input, and the other to be located on the negative real axis—one decade below the desired crossover frequency. The zero is normally located on the real axis within the range of 1/4 to 1/2 the frequency of the pole (Refs. 1 and 7). The zero position is selected to provide a phase boost for stability and for distinct frequency responses (i.e., initially faster time domain response due to the $G_d(s)$ crossover frequency and later a distinct slower response due to the zero frequency (Ref. 7). The location of the zero also influences the settling time of the control system response. Considering that MRC will be used later to force the control system response to follow that of the reference model, the zero location is chosen to be even closer to the pole location. Such a choice will speed up the settling time, while still preserving stability. Based on this and with additional mid-frequency gain considerations for noise attenuation including considerations for high frequency roll-off (Refs. 6 and 7), the desired OL TF for this design is

$$G_d(s)= 0.75\frac{(s/0.075+1)}{s(s/0.09+1)} \quad (3)$$

Here, the desired OL TF design has a proportional gain, $K_d = 0.75$, a pole at the origin, another pole at –0.09 rad/s, and a zero at -0.075 rad/s. The process outlined in References 1 and 7 for calculating the controller TF to match the Bode gain of $G_d(s)$ is also followed here with some deviation. Previously, padding poles were added when a zero was added to the design of the controller TF, $Gc(s)$, to keep the TF proper. The padding poles will not be added here, which will make the controller non-causal. However, the objective is to produce a combined controller and plant TF with $n_z = n_p - 1$. Without considering higher frequency unmodeled dynamics, if this controller were causal, this approach would make the control system infinitely robust to PPGU and robust to uncertainty for the rest of the plant dynamics. For more information on the robustness of such a design, see Reference 1 for the RL shape this design produces.

As outlined in References 1 and 7, the controller TF design process starts by using the zero and the poles of $G_d(s)$, as well as a controller proportional gain, $K_c = K_d/K_{po}$. The value for K_d is the proportional gain of $G_d(s)$ in Equation (3). That is, K_d=0.75 or 10 times the frequency of the zero of the desired OL TF design. This K_c gain is selected to obtain good performance for mid-frequency disturbance rejection. The gain K_{po} is the low frequency gain of $G_p(s)$ from Equation (1) (i.e., K_{po}=K_p*$89.57/2.875$), where $K_p = 1$ in this case (i.e., the value of K_p at the condition selected for design). Next, the 3 dB separation point between the Bode magnitudes of G_d and G_C*G_P is found and a pole or zero is inserted at this frequency into the controller TF in order to match their respective Bode gains and phases at higher frequencies. Here a zero is inserted because at this frequency point the magnitude of G_C*G_P is less than that of G_d. This process of finding 3 dB separation and inserting either zeros or poles is repeated until a satisfactory match is achieved up to or above the 0 dB crossover frequency of $G_d(s)$. Matching the magnitudes of G_C*G_P and G_d usually works out to also match their phases in terms of the desirable phase margin of the control system. If that is not the case, this matching process can be continued to higher frequencies. For this exercise, the matching continues until sufficient zeros are inserted in the control design (no padding poles) so that the TF of $G_{C*}G_P$ ends up with one less zero than pole. The result is an OL TF that includes the seven poles in $G_P(s)$ (Eq. (1)), and the two poles of G_d, for a total of nine poles. Therefore, the net number of zeros that will be needed for the non-causal controller TF is eight.

The Bode plot illustrated in Figure 1 shows the desired OL TF $G_d(s)$, and the TFs for $G_C(s)G_P(s)$ for eight sequential steps in the controller design process. The Bode plot for $G_d(s)$ is a blue trace at the top, overshadowed by the orange trace representing the 8th controller design (i.e., *Gc*8**Gp*). The orange trace at the bottom pertains to controller *Gc*1 (i.e., *Gc*1**Gp*), which is the first match attempt. Sequentially better matches can be seen with each successive step in the controller design up to and including the TF with the final controller design, *Gc*8**Gp.* The *Gc*8**Gp* match is very good (orange on top of blue line). By following the instructions provided, the final controller design step will have a zero placed at approximately 470 rad/s. Instead, this zero is placed at 250 rad/s to reduce the controller frequency, while achieving about the same objectives in terms of matching as described before. It can also be seen in this figure that the crossover frequency of the final OL design, *Gc*8*G_P, which influences the response time, is kept at approximately 0.9 rad/s as was originally desired. Not shown well within the plot resolution, is a mid-frequency disturbance rejection of approximately 20 dB. As can be seen by inspection of the *Gc*8**Gp* trace in Figure 1, the phase delay remains at about –90°. This means that the control system, while not accounting for the possibility of higher frequency unmodeled dynamics, is stable for infinite PPGU. This is so because no matter how much the proportional gain of the plant is changed, this phase margin is maintained. This design should also tolerate large variations in the rest of the plant dynamics as will be described later. The calculated controller TF (*Gc*8) from the design steps outlined above is as follows:

$$G_C(s)=\frac{1.989x10^{-11}s^8+1.336x10^{-8}s^7+2.9x10^{-6}s^6+2.297x10^{-4}s^5+7.656x10^{-3}s^4+0.1054s^3+0.4623s^2+0.355s+0.02407}{11.11s^2+s} \quad (4)$$

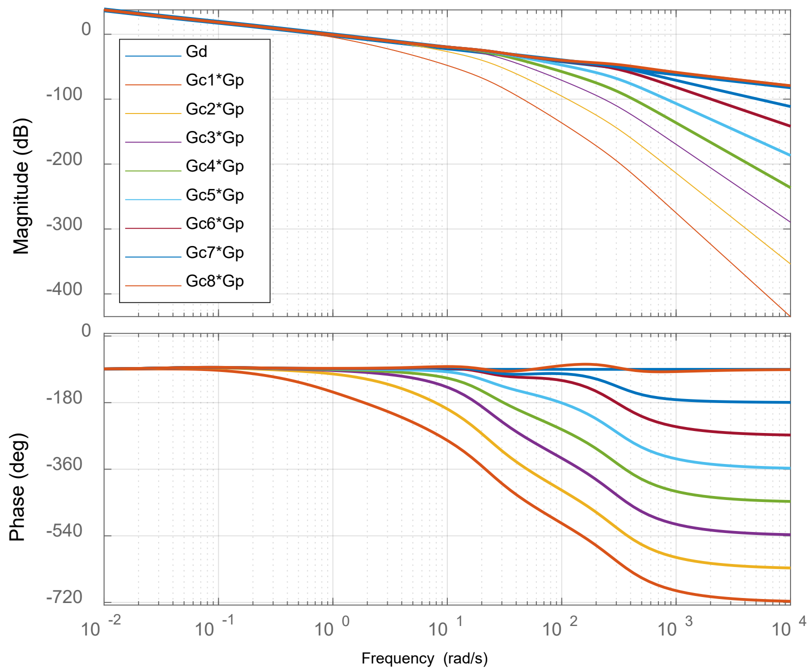

Figure 1.—Bode responses of the desired OL gain, $G_d(s)$ and those of the controller times the plant, $G_C(s)G_P(s)$, for successive controller design steps (Gc1 to Gc8).

By inspection, the Gc design is non-causal as expected. Since no padding poles were used for this non-causal controller design and without making any adjustments to the location of the zeros (as described above), the non-casual controller design could have simply been calculated as $G_c=G_d/G_p$. This simple calculation for the controller design stands to further simplify the non-causal controller design approach. The implied approach for direct cancelation of the plant poles and zeros can be problematic. For nonacademic cases, the precise location of the plant poles and zeros will not be known, or they can shift with time. If the controller cancellation zero or pole falls to the left versus to the right of the corresponding plant frequency, this can make a significant difference in the root locus trajectories and significantly affect the performance of the control system. However, with OL TFs of one less zero than pole, this will not be the case. The reason is briefly described in the next paragraph, with more details provided in Reference 1.

At this point, the resultant controller TF (Eq. (4)) for this exercise is improper. The RL for this non-causal controller design is shown in Figure 2. As shown in this figure and as described in Reference 1, a control system with this kind of RL shape will remain stable for all values of proportional gain greater than zero; because, all the RL paths have sufficient damping, which prevents oscillations in the response. Furthermore, as can be seen from this RL shape, independent of how the values of the existing plant dynamics are changed, the RL trajectories will stably remain in the left-half plane. Therefore, this design will be robust as long as there are no unmodeled plant dynamics that can change the difference between the number of zeros and poles of the OL TF. If there are unaccounted for plant dynamics, which is almost inevitable for sufficiently high frequencies, then the control system will still be stable or robust up to or near the proportional gain or control bandwidth where such frequencies are encountered. To demonstrate the stability properties of this design and its tolerance to uncertainty in the plant dynamics, a data point is selected in Figure 2 that represents a plant proportional gain of 403/0.75 = 537 times the plant proportional gain considered while designing the controller. For this plant proportional gain, the dominant

CL system poles have a damping of 0.747. This damping is close to the lowest damping on the RL trajectory for all values of proportional gain, which only amounts to a few percent overshoot. The feedback control design of the combined controller and plant TF are simulated with very high PPGUs. To illustrate this point, three step responses of the CL control system are shown in Figure 3. These traces verify the stability of the RL design shown in Figure 2 and the infinite robustness to PPGU, again, assuming there are no unmodeled plant dynamics. However, this control design is not physically realizable, except for cases where the controller and the plant TF can be combined in an analog fashion or an analog control design can be implemented, see Reference 1.

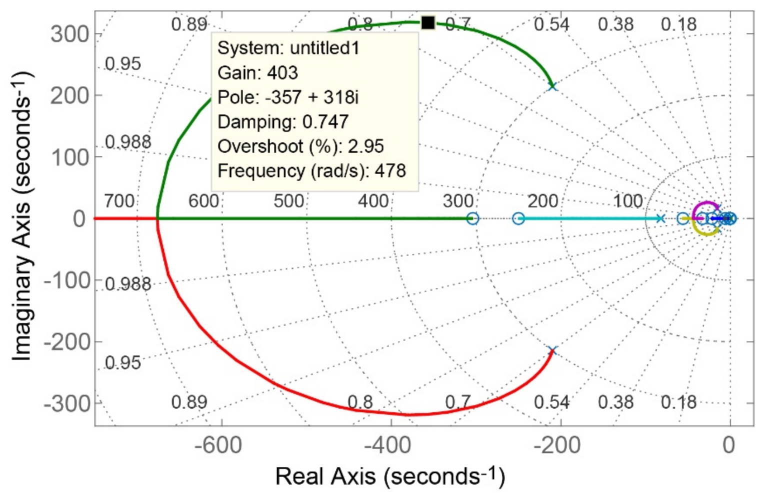

Figure 2.—Root locus trajectory of the non-causal control system design.

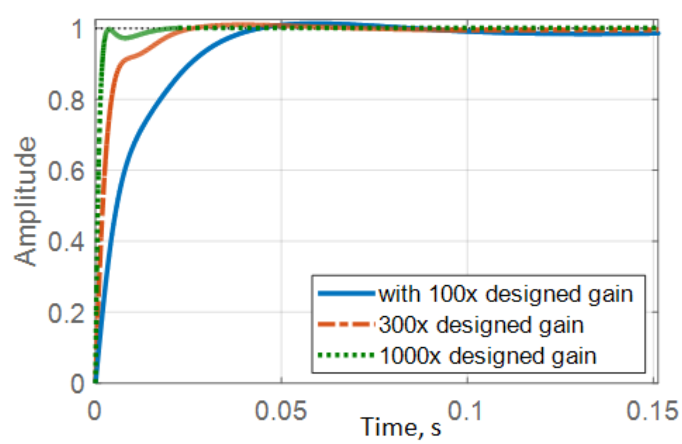

Figure 3.—Feedback control system responses with high plant proportional gain uncertainty.

2.3 The Non-Causal Controller Design

Since the controller TF in Equation (4) is improper, the next step is to calculate a causal approximation for this TF. First, the partial fraction decomposition of the improper TF is determined Reference 12. The partial fraction decomposition of Equation (4) results in a summation expression as follows:

$$G_C(s)= \frac{0.004214}{s+0.09} + \frac{0.02407}{s} + 1.790x10^{-12}s^6 + 1.2024x10^{-9}s^5 + 2.6092x10^{-7}s^4 + 2.0652x10^{-5}s^3 + 6.8725x10^{-4}s^2 + 9.4251x10^{-3}s + 4.0763x10^{-2} \quad (5)$$

As seen in Equation (5), there are six derivative terms that will need to be approximated using a proper TF. Derivative approximations can be created by constructing suitable LP filters. A first order filter design is used for the first order derivative with correspondingly higher order filters for higher order derivatives. This is done so that the resultant derivative TFs have a relative degree of zero. This avoids inadvertently adding more dynamics that may compromise the approximation. The form for the first order derivative approximation is as follows:

$$G_{S1}(s)= \frac{s}{\tau s+1} \quad (6)$$

A simulation diagram for this first order derivative approximation is shown in Figure 4, where K_1 is the proportional term of the first derivative in Equation (5) ($K_1 = 0.0094251$) and τ is the time constant of the LP filter for the approximation. Selecting a value for τ will be discussed later in this document. The second derivative term can be approximated by cascading the diagram shown in Figure 4, but with the output of stage 1 taken before the gain K_1 and connecting it to the input of stage 2. This cascading process from one derivative to the next is continued to form higher order derivative terms. The following is the resulting TF for the second order derivative approximation:

$$G_{S2}(s)= \frac{s^2}{(\tau s+1)(\tau s+1)} = \frac{s^2}{\tau^2 s^2+2\tau s+1} \quad (7)$$

As seen in Equation (7), the denominator on the right is written in the *normalized form* of a TF representation: $s^2/\omega^2 + 2\zeta s/\omega + 1$. By equating terms of the same order, the values for ω and ζ are: $\omega = 1/\tau$ and $\zeta = 1$. Since Zeta=1, this filter representation is *critically damped.* The higher order derivative approximations will also be critically damped, which is important for the accuracy of the complete approximation.

Figure 5 shows the complete simulation diagram for the causal approximation of the decomposed non-causal controller of Equation (5). A suitable value for tau can be selected based on the following considerations. A smaller value of τ permits higher controller rates and increased accuracy for the derivative terms for representing the original controller TF design in Equation (4) thus, resulting in increased robustness to PPGU. However, either smaller values of τ or robustness to higher PPGU (causing a proportional increase in the control system bandwidth), will require shorter sampling times. If control rate limiting is employed in the design and if it limits these higher controller rates, the performance may be compromised. Selecting a value for τ should be made in conjunction with a control or actuation rate limit. For a start, the value of τ can be selected so that the rate of the highest derivative in the controller, during a simulation, does not exceed the actuation rate limit.

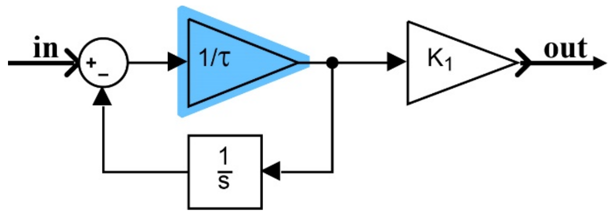

Figure 4.—Simulation diagram of the first order derivative approximation of Equation (6).

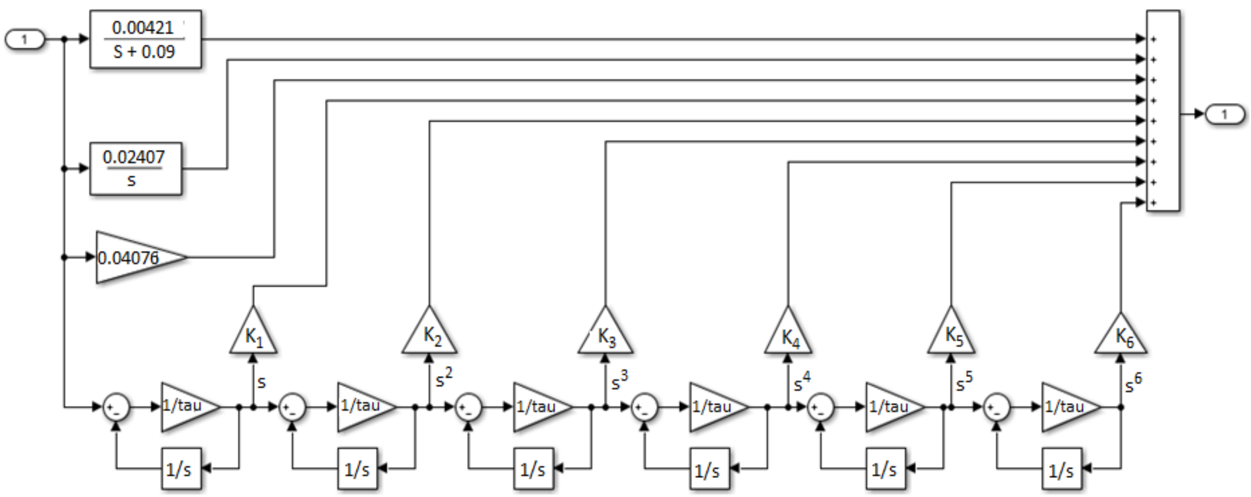

Figure 5.—Controller simulation diagram approximating the non-causal controller of Equation (5).

It is evident from the controller in Figure 5 that the second to the fourth summation elements from the left prescribe a Proportional Integral Derivative (PID) controller structure. As long as the non-causal controller TF has an integrator like the one shown in Equation (4), part of the control structure approximation will always turn out to include a PID. This new controller structure is more complex, and unlike traditional PID, tuning of the gains are not required. This process presents a precise methodology for determining the controller structure and for calculating the gains.

The controller structure shown in Figure 5, is used with the plant TF of Equation (1) in a feedback control system simulation to verify the robustness of the design. Step responses are illustrated in Figure 6 with different values of τ and with the plant proportional gain, K_p, set to 100. As expected, the smaller values of τ improve the performance as the response of the causal approximation approaches that of the non-causal controller. Similarly (not shown), this control system design can tolerate large uncertainty for the rest of the plant dynamics. For instance, for the plant proportional gain used for the design and for τ=1/2000, the plant frequencies can vary by many times their original values. Furthermore, at 100 times the designed proportional gain, plant frequencies can vary by ± 100 percent before performance deteriorates.

3.0 MRC Augmentation

The objective is for the control system response to meet that of the reference model of Equation (2) in lieu of the relatively large PPGU. This could be done by including a set-point filter (Ref. 13) but, here an MRC structure is chosen. In addition, the overall robustness of the non-causal controller and its MRC augmentation is demonstrated in this section.

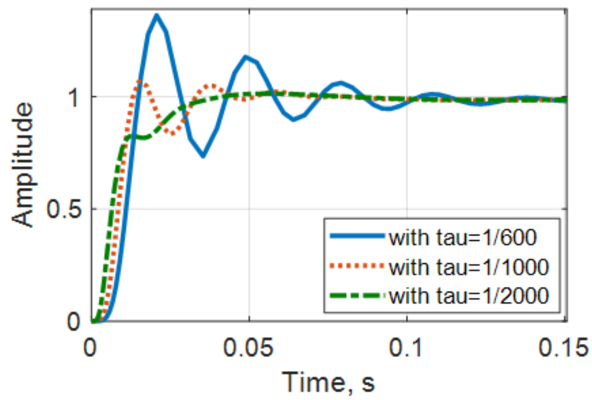

Figure 6.—Feedback control system responses for the causal controller design approximation shown in Figure 5 with 100x the designed proportional gain and for different values of τ.

The MRC structure employed here is shown in Figure 7. In Figure 7, the Controller block is the algorithm that is illustrated in Figure 5, the Plant is the TF (G_P) in Equation (1), the Reference Model is the TF (G_R) in Equation (2), and a limited band of white noise is introduced into the simulation. The Uncertainty Gain shown in Figure 7 is for testing PPGU. A gain of 1 signifies the plant gain used for control design. Time domain step responses for Uncertainty Gains of 0.01 and 100 are shown in Figure 8 and Figure 9, respectively. A LP filter design with a cut-off frequency below that of the OL cross-over frequency (to slow the response of the outer feedback loop compared to the inner loop) is added to the MRC feedback path shown in Figure 7 to decrease the frequency content of this signal. The filter helps to reduce oscillations introduced by the feedback path; thereby, improving the robustness of the design. The responses shown in Figure 8 and Figure 9 have $\tau = 1/2000$ and a MRC gain of 80 (see Figure 7). For these choices and for the LP filter design used, the trace in Figure 9 indicates an abrupt response at the point where set point switching takes place (green trace on top of blue trace). This short lived spike indicates that oscillations can be expected for plant gains that exceed 100x the plant gain used for the design. This conclusion is also supported by the response shown in Figure 6 for $\tau = 1/2000$. This degree of robustness significantly exceeds the initial objective of PPGU sought for this control system design.

The MRC structure guides the control system response to meet the reference model response for a large range of uncertainty in plant dynamics. For the expected PPGU range described earlier for the plant in Equation (1), the system responses will closely follow that of the reference model. The spike in Figure 9 for a PPGU of 100, can be attenuated by reducing the value of the MRC gain. However, a smaller MRC gain will slow down the response for PPGU<<1, like the response for the PPGU gain shown in Figure 8.

Noise rejection at one decade below the designed crossover frequency of the OL system is a typical measurement of performance (Refs. 1 and 7), which compares to approximately 20 dB for the basic LS feedback controller design. For the designed proportional gain and for $\tau = 1/2000$, the noise rejection of the MRC at 1 decade below the crossover frequency of 0.9 rad/s, is approximately 57 dB or about 700 times reduction. The crossover frequency is usually selected to make full use of the process actuator speed (Refs. 1 and 7). However, for this causal controller approximation, robustness can be compromised by taking that approach. This is because actuation rate limiting can affect the accuracy of the causal controller approximation. The noise attenuation results described here are not influenced by the LP filter that was included as part of the plant dynamics in Equation (2), because the corner frequency of that filter happens to be at a much higher frequency.

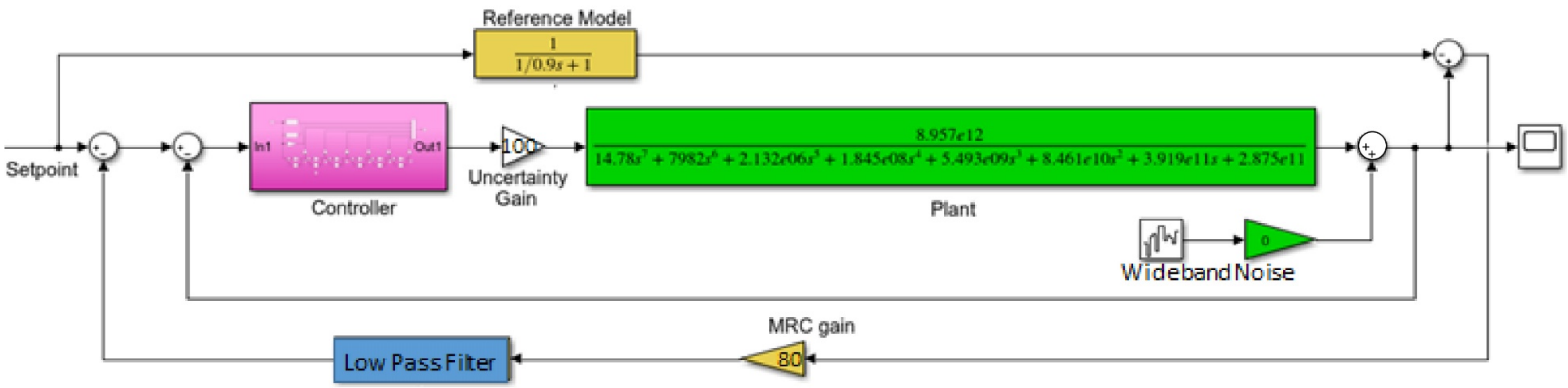

Figure 7.—MRC structure.

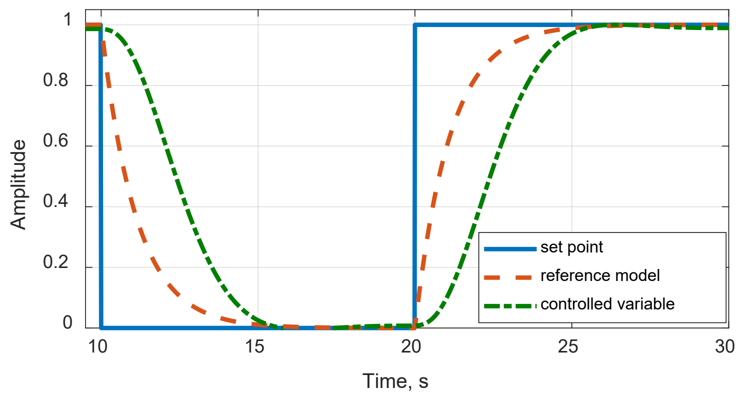

Figure 8.—Control system step response with a proportional gain equal to 0.01 times the designed gain.

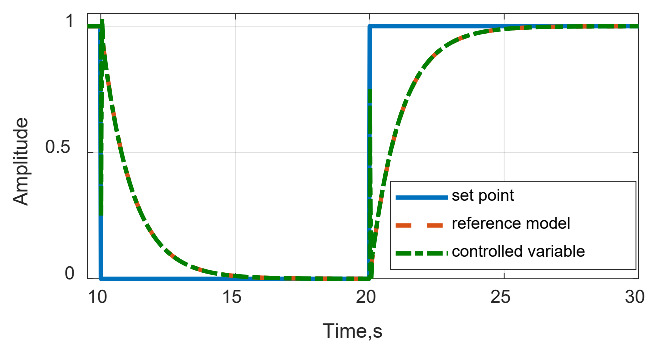

Figure 9.—Control system step response with a proportional gain of 100 times the designed gain.

The performance shown from these responses, for both the basic (Figure 6) and for the MRC designs (Figure 8 and Figure 9), illustrate the extent of the robustness of this control system design approach. The performance achieved with this design methodology is similar to that covered in Reference 6. The advantage of using this design approach is a simplified methodology. However, this approach may be limited in performance in terms of fully using the prescribed speed of the actuation system.

4.0 Conclusion

A new control design methodology is introduced in this paper using a non-causal controller design and a causal approximation. This control methodology usually culminates with a PID control embedded in its structure. However, unlike PID, this methodology follows a systematic controller design process based on a loop shaping approach that allows the gains of the causal controller approximation to be precisely determined. The robustness of this methodology to high plant proportional gain variability depends on the chosen derivative approximation time constant - with low values exhibiting more robustness while requiring faster sampling times. As illustrated in the paper, this control design can be augmented with a model reference control approach that allows the final control system design to exhibit desirable response time characteristics. At the same time model reference control augmentation can potentially significantly improve the robustness of the design. The overall design in the example presented can accommodate more than ± 2 orders of magnitude of plant proportional gain variability. In addition, this design approach considerably improves the system robustness to variations in the plant frequencies and damping. Robustness can be compromised; however, if due to the controller design or due to the variability in the plant dynamics, the limit of the actuator bandwidth is reached. This is because control or actuator rate limiting can impact the accuracy of the causal controller approximation.

References

1. Kopasakis, G., “Methodologies for Root Locus and Loop Shaping Controls design With Comparisons,” NASA/TM—2017-219721, Dec. 2017.
2. dos Santos, F.L.M., Gripp, J.A d-B., Filho, A.A., Luiz Góes, L.C.S., “Comparison of Robust Control Techniques for Use in Active Suspension Systems,” Section II – Control Systems, ABCM Symposium Series in Mechatronics, Vol. 5, pg. 270-279, 2012
3. Rotuno, M, Basso, M., Pome, A.B., and Sallusti, M. “A Comparison of Robust Attitude Control Techniques for a Solar Sail Spacecraft,” AIAA 2005-6083, AIAA Guidance, Navigation, and Control Conference and Exhibit, San Francisco, CA, DOI: 10.2514/6.2005-6083, August 15-18, 2005.
4. Navaro-Topia, D., Marcos, A., Bennani, S., and Roux, C., “Robust-Control-Based Design and Comparison of an Adaptive Controller for the VEGA Launcher,” AIAA 2019-0649, AIAA SciTech Forum, DOI: 10.2514/6.2019-0649, San Diego CA, January 7-11, 2019.
5. Wie, B., Bernstein, D.S., “Robust Controls Design for a Benchmark Problem, Journal of Guidance, Control and Dynamics,” Vol. 15, No. 5, DOI: 10.2514/3.56578, 1992.
6. Kopasakis, G., “A Robust Control Methodology via Loop Shaping, Root Locus, and Model Reference Control,” NASA/TM-20210010341, April 2021.
7. Kopasakis, G., “Feedback Control Systems Loop Shaping Design with Practical Considerations,” NASA/TM—2007-215007, Sept., 2007.
8. Agamennoni, O., Figueroa1, J.L., Desages, A.C., Palazoglu, A., Romagnoli, J.A., “A Loop-Shaping Technique for Feedback Control Design,” Elsevier Journal of Computer and Chemical Engineering, vol. 20, Issue 1, pg. 27-37, DOI: 10.1016/0098-1354(95)00007-O, 1996.
9. Gilev, B., “Wind Turbine Model and Loop Shaping Controller Design,” American Institute of Physics Conference Proceedings, vol. 1910, Issue 1, 2017, DOI: 10.1063/1.5013955.
10. Schinstock, D.E.; Wei, Z.; Yang, T.; “Loop Shaping Design for Tracking Performance in Machine Axes,” Elsevier Journal of International Society of Automation (ISA) Transactions, vol. 45, no. 1, pg. 55-66, DOI: 10.1016/s0019-0578(07)60065-2, 2006.
11. Taylor, J.D., Gentilini, I., and Mesner, W. “Loop-Shaping Controller Design for Nonlinear Systems Using the Contoured Robust Controller Bode (CRCBode) Plot,” American Control Conference, Fairmont Queen Elizabeth, Montreal, Canada, June 27-29, 2012.
12. DeRusso, P.M., Roy, R.J., Close, C.M., “State Variables for Engineers,” 2nd edition, John Wiley & Sons, Inc, pg. 116-118, 1998.
13. Kopasakis, G; “An Innovative Feedback Controls Design Approach for Aero Engines,” NASA/TM—2019-220361, Nov., 2019.